Tikrit Journal of Engineering Sciences (2024); 31(3): 44-59
DOI: http://doi.org/10.25130/tjes.31.3.5

IRAQI Academic Scientific Journals

ISSN: 1813-162X (Print); 2312-7589 (Online)
Tikrit Journal of Engineering Sciences
available online at: http://www.tj-es.com

TJES Tikrit Journal of Engineering Sciences

MnO_2 Nano Particles Modified a Double Layer Cathode Reactor for an Efficient Removal of DBT in Diesel

Maha Nazar Ismael [a,b] *, **Ghassan H. Abdullah** [d], **Hatem Mhiri** [c], **Fatin Hassan Yahya** [b]

a National School of Engineering of Gabes, University of Gabes, Gabes, Tunisia.
b Department of Chemical Engineering, College of Engineering, Tikrit University, Tikrit, Iraq.
c National School of Engineers of Monastir, Laboratory of Thermal and Thermodynamic of Industrial Processes, Monastir, Tunisia.
d Department of Petroleum and Gas Refining Engineering, College of Petroleum Processes Engineering, Tikrit University, Tikrit, Iraq.

Keywords:
Deep Desulfurization; MnO2 Nanoparticles; Polytetrafluoroethylene; Cathodic Reduction; Dibenzothiophene.

Highlights:

- MnO2 synthesis using co-precipitating method.
- Electrochemical reactor modification using MnO2-PTFT as a cathode.
- Electrochemical Diesel desulfurization.
- Study Desulfurization Reaction Kinetics.

ARTICLE INFO

Article history:

Received	26 Jan.	2024
Received in revised form	26 Mar.	2024
Accepted	17 Apr.	2024
Final Proofreading	01 June	2024
Available online	03 July	2024

Citation: Ismael MN, Abdullah GH, Mhiri H, Yahya FH. **MnO_2 Nano Particles Modified a Double Layer Cathode Reactor for an Efficient Removal of DBT in Diesel**. *Tikrit Journal of Engineering Sciences* 2024; **31**(3): 44-59.
http://doi.org/10.25130/tjes.31.3.5

*Corresponding author:

Maha Nazar Ismael
National School of Engineering of Gabes, University of Gabes, Gabes, Tunisia.

Abstract: Due to its many engineering applications, low manufacturing costs, and environmental friendliness, 3D printing is considered one of the most promising manufacturing technologies. The quality of printed parts will inevitably be affected by the controllable variables used in the 3D printing process. The present study aims to investigate how different printing process parameters affect the bending strength of PLA prints. The ASTM D790 standard was used to fabricate the samples in this work, while the Taguchi principle was used to design the experiments. The following values were chosen: shell width (0.8, 1.2, 1.6, and 2 mm), layer thickness (0.15, 0.2, 0.25, and 0.3 mm), and infill density (40%, 60%, 80%, and 100%). The results showed that fill density is the most effective variable for improving bending strength. Measurements of infill density (100%), layer thickness (0.15 mm), and shell width (2 mm) gave the best results, which were calculated to be 83.1479 MPa in bending test. The mathematical model in this study was developed using linear regression analysis, and the residuals confirmed that the model fit the data well, with a maximum error of 6.1%.

ثنائي اوكسيد المنغنيز ككاثود ثنائي الطبقة لمفاعل مطور لإزالة فعالة لدايبنزوثايوفين من وقود الديزل

مها نزار إسماعيل [١،٢]، غسان حمد عبدالله [٤]، حاتم مهيري [٣]، فاتن حسن يحيى [٢]

[١] المدرسة الوطنية للمهندسين بقابس /جامعة قابس/ قابس - تونس.

[٢] قسم الهندسة الكيمياوية/ كلية الهندسة/ جامعة تكريت/ تكريت – العراق.

[٣] مختبر الحرارة والديناميك الحراري للعمليات الصناعية /المدرسة الوطنية للمهندسين في المونستير/ المونستير - تونس.

[٤] قسم تكرير النفط والغاز/ كلية هندسة العمليات النفطية / جامعة تكريت/ تكريت – العراق.

الخلاصة

بيروكسيد الهيدروجين هو عامل مؤكسد قوي لديه القدرة على أكسدة مركبات شوائب الثيوفين الموجودة في وقود الديزل. تركز هذه الدراسة على دراسة المفاعل الكهروكيميائي (TBER) لغرض إزالة الكبريت من الديزل. يتم تعزيز TBER من خلال استخدام محفز كهربائي عالي الكفاءة، وهو جسيمات نانوية MnO_2 منتجة خصيصًا، لتسهيل إنتاج بيروكسيد الهيدروجين في الموقع. تم تصنيع الجسيمات النانوية MnO_2 بطريقة الترسيب المشترك، ثم تم دمجها لاحقًا مع PTFE لإنشاء طبقة الكاثود. تم استخدام XRD وSEM وFTIR لفحص المحفز المنتج. يُظهر TBER أكسدة محسنة بشكل ملحوظ للثنائي بنزوثيوفين (DBT) في الديزل الذي يمر عبر TBER باستخدام إلكتروليت قلوي. نجح المفاعل الكهروكيميائي المحسن تصميمه في تحقيق أكسدة كاملة في الموقع لـ ٥٠٠ جزء في المليون من DBT خلال ساعتين، مما يدل على مستوى عالٍ من الكفاءة في إزالة الكبريت العميق من وقود الديزل.

الكلمات الدالة: ازالة كبريت عميقة، ثنائي اوكسيد المنغنيز النانوي، أوكسجين، بولي تترافلوروأثيلين، إختزال كاثودي،دايبنزوثايوفين.

1.INTRODUCTION

Crude oil contains several natural organic components, including organosulfur compounds. Petroleum products that have undergone refinement, such as gasoline, diesel, and aviation fuel, mostly consist of these molecules [1]. Sulfur dioxide (SO_2) and sulfate are byproducts of burning fuels that contribute significantly to air pollution and acid rain. Due to the significantly higher difficulty in improving heavy, sulfur-containing oil compared to light feeds, the oil price is inversely proportionate to its sulfur content. To regulate the amount of sulfur in fuels, some nations have passed legislation; for example, the United States has set a limit of 15 parts per million for diesel fuel [2,3]. Recently, Mno2 nanoparticles have been employed in desulfurization. A study conducted by Sadeghi and Hosseini [4] focused on examining the efficacy of a nano MnO2/Zeolite AgY composite and MnO2 nanoparticles in the adsorption and degradation of the 2-CEPS molecule. The synthesized composite of 15.8 wt% nano MnO2/AgY(2) exhibited adsorption and destruction efficiencies of around 66% and 84% for 2-CEP, respectively, for 10 hours. However, the concentrations of MnO2 nanoparticles were comparatively lower. Then, Yu et al. [5]. synthesized and investigated supported α-MnO2 nanosheets. The supported catalyst exhibited a notable level of desulfurization efficiency when used to remove DBT from a model oil, which was achieved by utilizing 30 wt% H2O2 as the oxidant while maintaining mild conditions. The removal efficiency of DBT in model oil with a sulfur content of 500 ppm was 97.7% at a temperature of 50 °C. Alheety et al. [6] used manufactured MnO2 nanoflowers to eliminate sulfur-containing compounds from simulated and actual diesel fuel samples. Additional enhancements to the ideal conditions for removing sulfur revealed that the diesel model obtained an oxidative desulfurization (ODS) rate above 95% using 0.5 g, 35 minutes, 60–62 °C, (O/S) 4, and 900 rpm. A range of metal-containing ionic liquid complexes and metal oxide-based nanocatalysts, including MnO2, α-Fe2O3, and Co3O4, have been effectively synthesized and utilized in oxidative desulfurization (ODS) of dibenzothiophene (DBT) [7]. Finally, MnO2 nanoparticles were cultivated on UiO-66 to produce a composite material known as MnO2/UiO-66 using the solvothermal process described by Subhan et al. [8] Compared to the original MOF, the MnO2/UiO-66 composite exhibited reduced particle size; increased surface area and pore volume; enhanced crystallinity, active Mn^{4+}, Mn^{3+}, and Zr^{4+} species; decreased binding energy for Zr, Mn, and O species; and heightened O– O interactions. These variables led to the rapid (3 min) and highly effective (100%) performance of DBT and pyridine in the ODS and ODN processes at 25 °C. This performance was achieved using an O/S and O/N ratio of 4 (each) and a catalyst dose of 0.06 g/15 mL (2000 ppm), with activation energy values of 6.2 kJ/mol and 6.8 kJ/mol, respectively. Recently, hydrodesulfurization (HDS) is the method of choice for desulfurization. However, this method can only reduce the sulfur concentration to a few hundred parts per million [9]. This technique necessitates intense working conditions, including high temperatures and pressures, drastically decreasing sulfur content. Benzothiophene (BT), dibenzothiophene (DBT), and its derivatives are extremely expensive and energy-intensive to remove, and these conditions are necessary to do so. This HDS method is believed to create ultra-low sulfur diesel under extremely harsh conditions [10,11]. A graphene catalyst based on cobalt and molybdenum oxides (CoMo/G) was investigated for heavy naphtha

hydrodesulfurization, and the results indicated a sulfur removal efficiency of 79% [12]. In addition, accumulating three promoter metals has the potential to enhance the traditional catalysts' performance, which would be a major step forward for HDS and ODS procedures [13-18]. Nonetheless, other alternatives to hydrodesulfurization were explored for OSC elimination, including oxidation [19], extraction [20], adsorption [21], and biodesulfurization [22]. Activated carbon and a Zr-based UiO-66 molecular organic framework for enhanced fuel treatment procedures, such as adsorptive and oxidative desulfurization and denitrogenatation, were recently created using nanoparticles of zinc, manganese, and manganese dioxide [8, 23]. Numerous scholars have suggested electrochemical oxidative desulfurization as a novel class of desulfurization [24,25]. Reactive oxygen may be efficiently generated using electrochemical desulfurization [26]. This method exhibits little oxidant use and generates minimal wastewater, making it highly valuable for study in fuel technology [27]. Schucker and Baird [28,29] suggested an electrochemical oxidation technique for desulfurizing naphtha, whereby the resulting sulfones may be readily eliminated using polar solvents. Chen et al. [30] experimentally assessed the efficacy of an electrochemical method utilizing a NaCl electrolyte solution for removing sulfides in coal. Wang et al. [31,32] used a fluidized-bed electrochemical reactor with a catalytic anode made of (β-PbO_2/C or CeO_2/C) to purge gasoline of organic sulfur compounds. Liu et al. [33] examined an electrochemical oxidation procedure in a ternary solution comprising acetonitrile, alcohol, water, and acetic acid to eradicate DBT in a targeted oil sample. They found that the highest conversion percentage for DBT was 98.4%. González-Fuentes et al. [34] created a catalyst composed of three metals, i.e., IrO2, SnO2, and Sb2O3, to remove sulfur from DBT. Tang et al. [35] used a combination of electrochemical oxidation and solvent extraction to remove organic sulfide from condensate gasoline. A desulfurization efficiency of 99.62% was reached under ideal operating circumstances and with three extraction phases. Finally, Yaseen et al. [36] investigated the oxidative desulfurization of DBT in transportation fuels using NaClO utilizing a novel catalyst composed of Cu and Ni on activated carbon derived from banana peels. The newly developed catalyst-oxidant system was praised for its efficiency, low cost, and positive outcomes. Most of these procedures involve direct electrochemical oxidation desulfurization methods, which need organic electrolytes with large overpotentials.

The trickle-bed electrochemical reactor (TBER) has been demonstrated as a viable electrochemical method for the on-site oxidation of DBT [37]. This study explores the potential for enhancing the efficiency of the TBER in generating H_2O_2 and oxidizing DBT in situ. In addition, utilizing MnO_2 as a novel catalyst, in conjunction with polytetrafluoroethylene, was applied to augment the rate of H_2O_2 formation and facilitate the in situ oxidation of DBT in diesel fuel. Additionally, an examination was conducted on a change in the TBER design, whereby two rows of eight holes were employed rather than a single row to distribute the electrolyte throughout the unique Mno2-ptfe cathode evenly. The improved TBER achieved total desulfurization efficiency by generating in situ oxidants, i.e., H_2O_2, and oxidizing DBT.

2.EXPERIMENTAL METHOD

2.1.Materials

The components purchased from Sigma-Aldrich include PTFE aqueous suspension (60 wt % dispersion in water), 85% KOH, $KMnO_4$, $MnSO_4$, dibenzothiophene DBT, and molybdic acid $(NH_4)_6Mo_7O_{24}•4H_2O$. The H_2SO_4 (98%) molecules were obtained from Alfa Aesar. The electrolyte solution for each experiment was prepared using deionized water of the utmost grade.

2.2.Trickle Bed Electrochemical Reactor (TBER)

All experiments were conducted using the TBER experimental design shown in Fig. 1. Meanwhile, Fig. 1 (a) shows that the modified cathode frame can find one gas inlet and two solution inlets on top of the cathode housing. The liquid was evenly distributed over both cathode beds by drilling two rows of eight holes. A specific intake allows oxygen to enter the system. This intake is installed in the gap between the two frame-side MnO_2-PTFE-SSM cathode beds. The uniform oxygen distribution was achieved using the MnO_2-PTFE pads, which were 1 cm thick [38]. There are two outlets for the passage of products and unreacted materials from the two sides of the reactor combined in one outlet to the solution tank at the base of the apparatus. On the other hand, Fig. 1 (b) shows all the layers of TBER, stainless steel anodes, and meshes SSM (layers 1 and 3) measuring 7 by 6 cm with a 1 mm mesh size, which were part of the revised design. Enclosing the reactor components with 12 cm broad, 11 cm high, and 2 cm thick plastic panels (layer 4), and finally (layer 2) a rubber piece to prevent a shortcut. To desulfurize DBT in diesel using a KOH electrolyte solution, the electrochemical reactor was designed with a continuous flow from the top downwards, utilizing a two-layer MnO_2-PTFE to composite cathode Fig. 2. A DC system (6), an oxygen cylinder (9), a three-necked flask (7), a pump (4), a water bath (8), and oxygen and liquid flow meters (2 and 3) were all part of the

experimental setup. A trickling bed electrochemical reactor (TBER) was also used (1). An electrical controller (5) was locally designed to regulate the pump's output because the liquid flow meter could not handle the pump's high pumping capability. Gas was pumped into the gas feeder chamber that separated the cathode beds to maximize oxygen diffusion on both sides of the catalyst beds. The electrolytes were poured over the MnO_2-PTFE beds from above the cathode frame. The voltages required to run the TBER reactor came from a direct current (DC) power source. The reactor's base emptied into the accumulation flask, where the unreacted materials were recirculated.

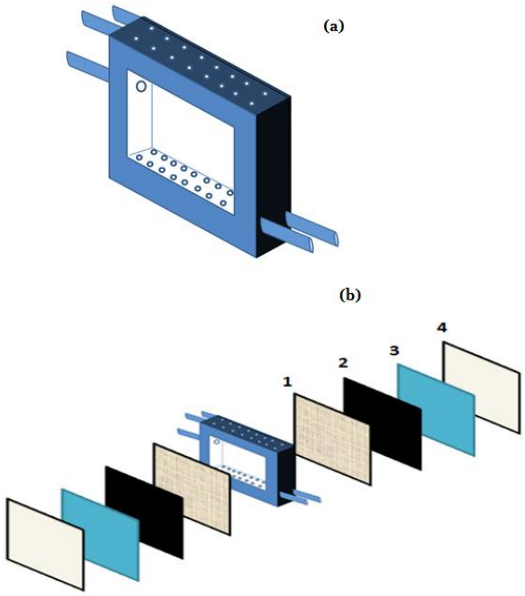

Fig. 1 (a) Schematic Diagram of Cathode Frame (b) Schematic Diagram of the Developed TBER Components.

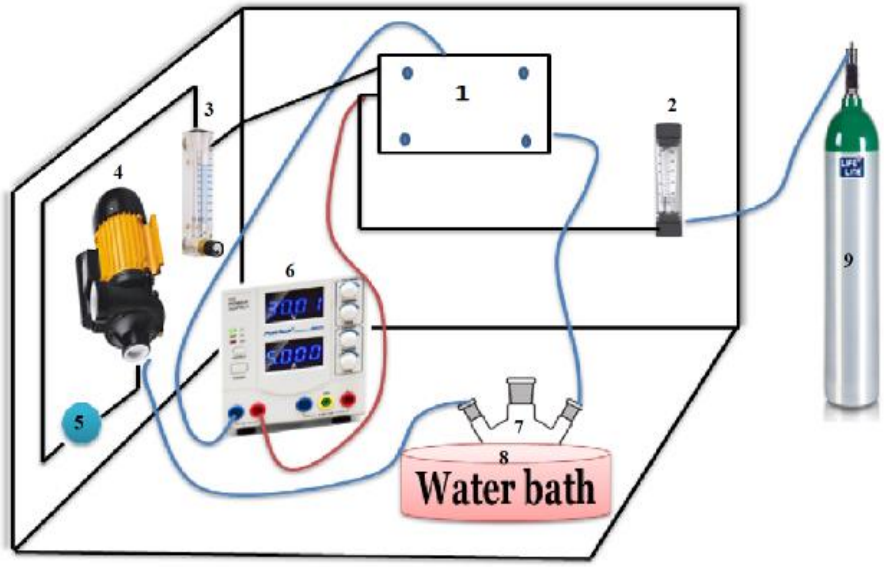

Fig. 2 Process Diagram for TBER, 1. TBER 2.O_2 Flow Meter 3. Liquid Flow Meter 4. Pump 5. Controller 6. Power Supply 7. Three Conical Flask 8. Water Bath 9. O_2 Cylinder.

2.3.Metal Oxide Nanoparticle Production (MnO_2)

The MnO_2 nanoparticles were prepared using the co-precipitation technique. The standard ingredients were 0.17 g of $KMnO_4$, 0.25 g of $MnSO_4$, and 10 mL of distilled water [39]. A homogenous solution was formed by mixing the ingredients under magnetic stirring for three hours [40] at 60 °C [41]. Following filtration via micro filters and washing with distilled water, the precipitates were dried overnight at 100°C. Lastly, they were calcined for two hours at 500°C [42]. The produced catalysts' characteristics were examined using XRD, SEM, and FTIR.

2.4.Diesel Desulfurization

Combining diesel with or without organ sulfur components with an electrolyte solution of KOH made it possible to use a two-fluid phase flow to investigate in situ sulfur oxidation by H_2O_2. Here, the porous cathode bed cells were used to mix and flow diesel fuel with and without DBT, as well as a 0.25 M KOH solution. Electrolyte bubbles supplied oxygen to the TBER Fig. 2. To enhance oxygen mass transfer and increase its concentration at the electrode-electrolyte interface, molecular oxygen is necessary. The original production of H_2O_2 was conducted without DBT to determine if it could be done using diesel.

2.4.1.H_2O_2 Concentration Measurement

A peroxymolybdate technique was used to test the concentrations of the H_2O_2 created [43]. Samples were prepared by mixing 0.5 mL of the solution with 5 mL of (2.4 mM) $(NH_4)_6Mo_7O_{24}$ in 0.5 M H_2SO_4. To measure H_2O_2 concentrations, a Genesys 20 spectrophotometer that operates at 300 nm was used. The following equation, based on Beer's law, can be used to determine the H_2O_2 content in the sample:

$$C = \frac{K}{V_{sample}} A_{300} \quad (1)$$

C: The H_2O_2 concentration (g/L)
V_{sample}: The sample volume (5 ml)
K: constant factor equal to 0.474 mg
A_{300}: The absorbance at 300 nm

2.4.2.DBT Concentration Measurement

To investigate sulfur oxidation by on-site H_2O_2 produced in the TBER, diesel fuel containing DBT was utilized. X-ray Fluorescent Energy Dispersive Sulfur Analyzer ASE-2, ED-XRF, was used to determine the DBT quantity in the diesel; begin by appropriately preparing the sample and ensuring that it was free from impurities and devoid of moisture. The device should be calibrated using established sulfur standards to produce precise readings. The analyzer was activated, and parameters were configured, such as excitation, and detector settings, according to the instructions provided by the manufacturer. Position the prepared sample into the analysis chamber and begin the analysis procedure with the software provided by the device. To ascertain the sulfur concentration, it is necessary to analyze the produced spectra, analyze the distinctive X-ray fluorescence emitted by sulfur atoms, and document and communicate the findings, including pertinent sample details and analytical parameters.

3.RESULTS AND DISCUSSION

3.1.Characterization of MnO_2 Nanoparticles

3.1.2.X-ray Diffraction (XRD) Test

XRD analysis of manganese dioxide nanoparticles produced using the co-precipitation technique is presented in Fig. 3. High-resolution multipurpose Theta/Theta XRD devise / Kashan laboratories was used. The XRD pattern clearly demonstrated that the synthesized manganese oxide nanoparticles were completely crystalline. It was found that manganese oxide nanoparticles had an average particle size of between 38 and 55 nm. This range is close to what Kahattha and Santhaveesuk [44] found. They studied the influence of calcination temperature on MnO_2 characterizations and found that the average particle size was 38 nm. Scherrer's equation states that 42 nm is the optimal size for MnO_2 nanoparticles to achieve maximum intensity: Debye-Scherer equation

$$D = \frac{0.98\lambda}{\beta_{0.5}\cos(2\theta)} \quad (2)$$

where λ represents the wavelength of the radiation being utilized, and $\beta_{0.5}$ refers to the width of the peak with the highest intensity at half its height.

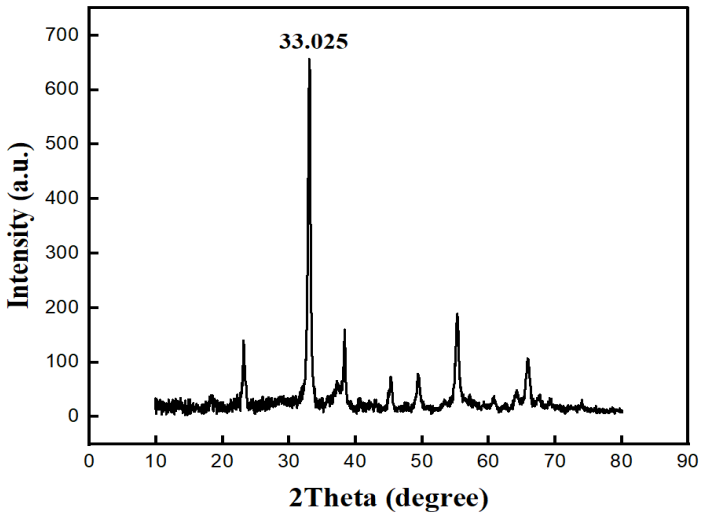

Fig. 3 X-ray Diffraction Pattern of Manganese Dioxide Metal Nanoparticles Synthesized by Co-Precipitation Method.

3.1.2.Fourier Transform Infrared (FT-IR) Test

Functional groups and other pollutants were identified using FT-IR spectroscopy. Hydrogen-bonded water molecules and hydroxyl groups on the surface of the sample were first thought to be responsible for the stretching vibrations seen in the wide band at 3344 cm^{-1} in Fig. 4. Additionally, the bands at 1631.83 cm^{-1} and 1105.24 cm^{-1} suggested the O-H vibrating mode of residues adsorbed water, which correlates to the existence of a large number of leftover hydroxyl groups. The MnO vibrations of the MnO_2 nanopowder were responsible for the band at 532.37 cm^{-1}. The organic groups present in MnO_2 nanoparticles were invisible in the spectrum. This test is consistent with the findings of Ganeshan et al. [45].

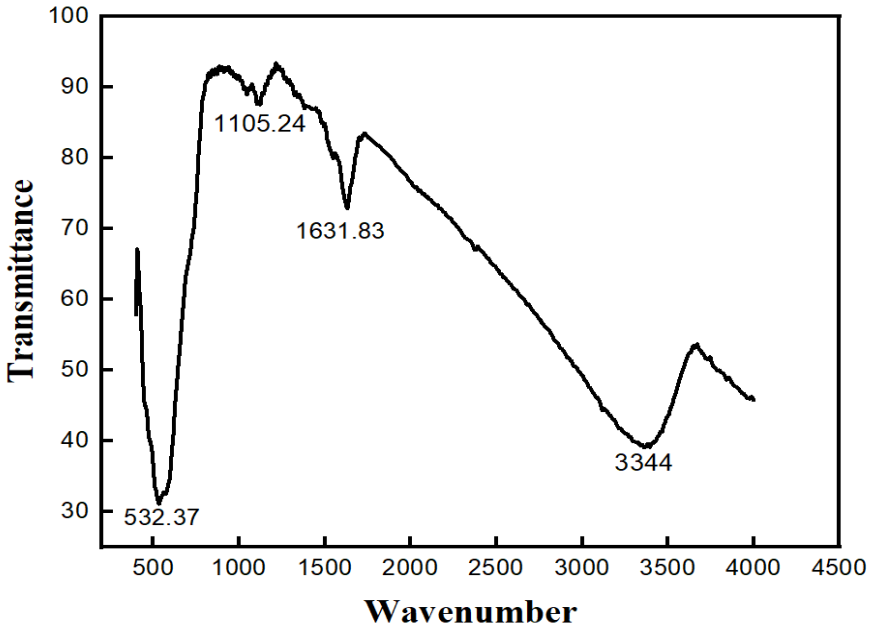

Fig. 4 FT-IR Spectra of Manganese Dioxide Metal Nanoparticles Synthesized by Co-Precipitation Method.

3.1.3.Scanning Electron Microscope (SEM) Test

Manganese dioxide (MnO_2) crystal structures exhibited a diverse range due to several corners and/or edges that share configurations among the building block units [46]. SEM photos at various magnifications are shown in Fig. 5. The observed powder exhibited two distinct shapes: small tubes, as depicted in Fig.5 (a), and clusters, as illustrated in Figs. 5 (b) and (c). These shapes have a notable inclination towards agglomeration, primarily attributed to their high surface energy, forming a substantial surface area. This irregular agglomerated form resembles the findings of Athar [47], who synthesized cubic MgO nanoparticles using a non-aqueous sol-gel. The larger particles can be attributed to the Ostwald ripening process, characterized by limited porosity and crystallinity. The particles had nearly a spherical shape and were uniform in size, with an average of around 39 nm, which is near what Ganeshan et al. [45] found.

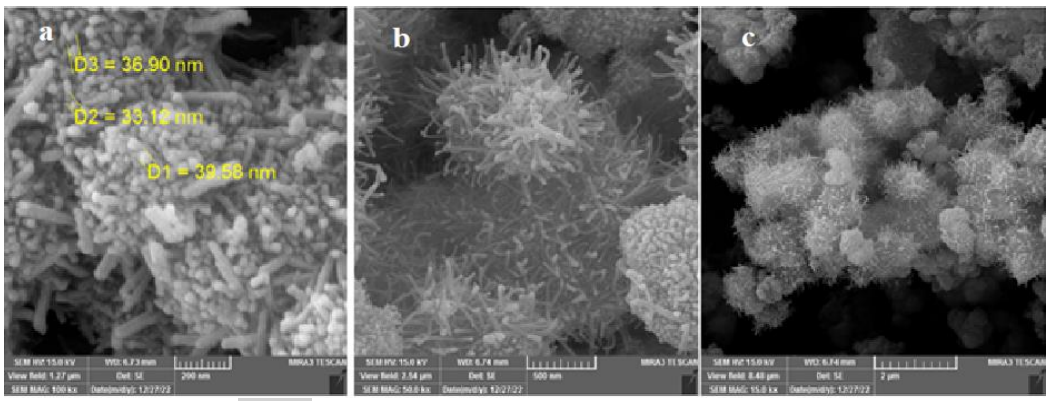

Fig. 5 SEM Micrographs of Mno_2 Nanoparticles.

3.2.Diesel with Dibenzothiophene in the Context of Hydrogen Peroxide Synthesis

Forming H_2O_2 in alkaline media occurs by an electrochemical process that proceeds via a two-electron route. In this process, oxygen (O_2) undergoes electrochemical reduction to generate peroxide ions (HO_2^-) as an intermediate. Subsequently, the peroxide ion accumulates in the solution and undergoes a chemical reaction to produce hydrogen peroxide (H_2O_2), as seen in Eqs. (3) and (4) [48].

$$O_2 + H_2O + 2e^- \longrightarrow HO_2^- + OH^- \quad (3)$$

$$HO_2^- + H_2O \longrightarrow H_2O_2 + OH^- \quad (4)$$

The produced hydrogen peroxide will oxidize sulfur atoms found in organic sulfur compounds. In steps 5 and 6, it was observed that the oxidation reaction produced sulfoxide of DBT ($C_{12}H_8S$) molecules in one step and sulfones in two steps [49].

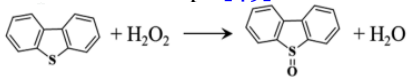

(5)

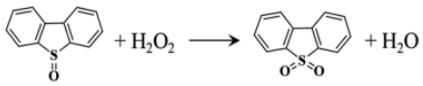

(6)

The oxidized sulfur molecules possess a significant degree of polarization, enabling their separation from diesel fuel by solvent extraction methods. Fig. 6 displays the results of hydrogen peroxide formation when diesel and diesel with DBT were added. In less than one hour, a 36.65 mm H_2O_2 concentration was produced utilizing a diesel-free electrolyte. The concentration dropped to 18.32 mm at the same time when 10% diesel by volume was used in the electrolyte. The non-conductive fuel in the electrolyte may mainly cause a reduction in H_2O_2 concentrations. Because diesel reduces the catalyst surface area that the aqueous phase occupies, it lowers H_2O_2 electro-generation. An increase in the time diesel is in contact with the catalyst surface due to its higher viscosity might reduce oxygen diffusion and charge transfer, resulting in poor H_2O_2 production. Gas phase oxygen flowed quickly, covering the catalyst MnO_2, which may explain why the high viscosity insignificantly affected the liquid hold-up in the bed [50,51]. A known quantity of DBT dissolved in diesel showed a small linear drop in H_2O_2 concentration with time. In less than an hour, the concentration peaked at 6.62 mM. Two mechanisms, its utilization in the oxidation of DBT and electrogeneration of hydrogen peroxide, were responsible for this reduction in peroxide production. The excess hydrogen peroxide concentration in diesel with DBT indicated that the created hydrogen peroxide did not wholly react with DBT, as shown in Fig. 6, which compares the three curves depicting the process of H_2O_2 formation. At the outset, the dissolved DBT concentration was 500 ppm (500 mg/L). In theory, 1000 mg/L of H_2O_2 would be required for its oxidation, suggesting that a process governed by diffusion occurred at the interface between the water and oil phases. For the sulfur species to undergo oxidation by the generated H_2O_2, they must spread to the contact. Complete oxidation of the organic Sulphur component necessitates circulating the diesel and the aqueous electrolyte.

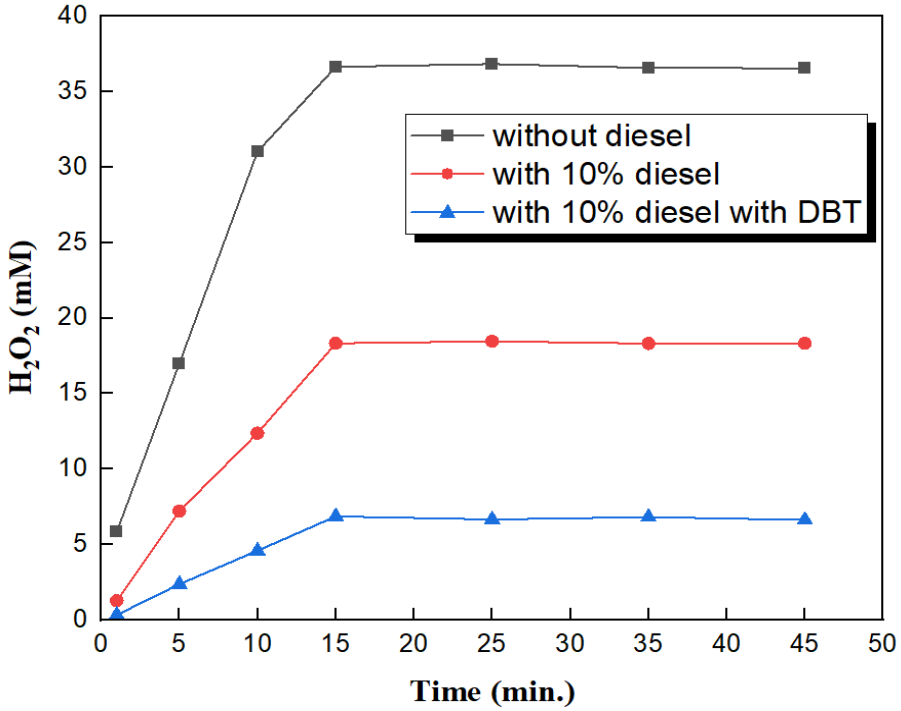

Fig. 6 (a) H_2O_2 Production as a Function of Diesel-Free Time Using 10% Diesel and 10% Diesel with DBT at Electrolyte and O_2 Flow Rates of 0.25 M KOH, 0.5 V, 15 ml/min, and 1.5 L/min at 20 °C.

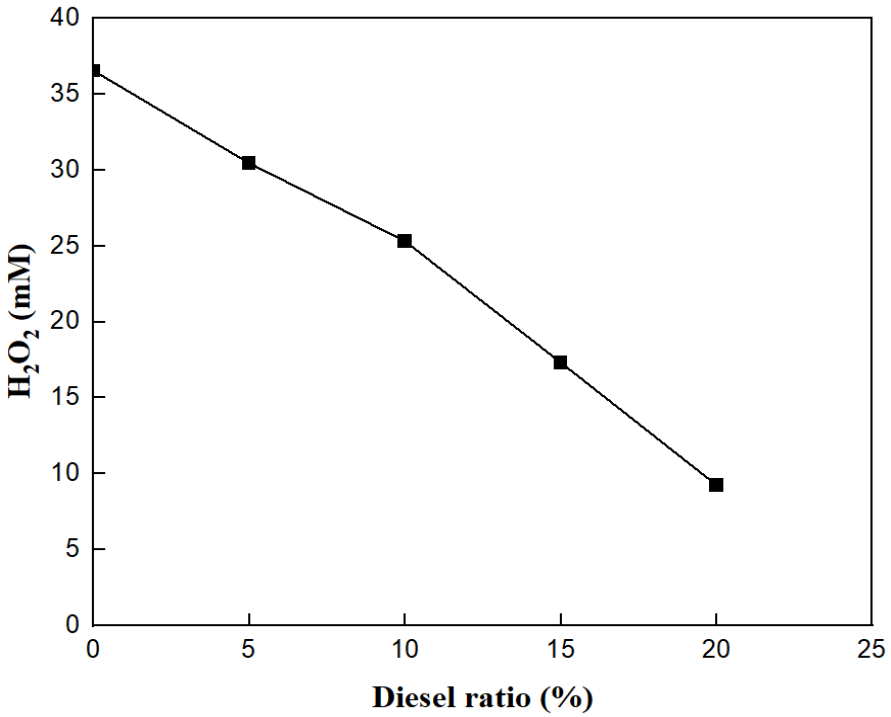

Fig. 7 The Relationship between Diesel Ratios and H_2O_2 Concentration.

3.3.Relationship Between Diesel Ratios and H_2O_2 Concentration

To conduct a more in-depth analysis of the impact of diesel, different diesel concentrations of 5, 10, 15, and 20% were utilized. The resulting concentrations of electro-generated H_2O_2 are displayed in Fig. 7. Producing H_2O_2 was reduced fairly linearly as the volume percentages of diesel grew. This outcome was anticipated as more diesel would effectively spread over the MnO_2 surface, reducing oxygen transportation to the reaction sites. MnO_2 has low hydrophilicity, resulting in the potential for its surfaces to be coated by the oil phase. Furthermore, the charge-transfer mechanism would experience a deceleration due to the non-conductive nature of the oil phase. The results of Fig. 7 align significantly with those found by Abdullah and Xing [52], with a reduction in stabilization time from 60 minutes to 15 minutes, which can be attributed to the effectiveness of the manufactured nanocatalyst MnO_2, compared to the carbon used in the study above.

3.4.DBT Oxidation Using in Situ-Generated Hydrogen Peroxide

Figure 8 displays the data that shows using H_2O_2 over time. It was observed that the H_2O_2 content did not change when diesel was utilized without DBT during the electrolysis process, suggesting that no consumption occurred. In contrast, the concentration of H_2O_2 decreased gradually throughout the first 50 minutes when diesel was mixed with extra DBT. The reaction between H_2O_2 and DBT in diesel is demonstrated by the concentration reduction, which goes from 18.32 to 6.62 mM. It was within 60 minutes that the maximum degree of oxidation was reached, as the curve started to approach equilibrium after 50 minutes. Using hydrogen peroxide in oxidizing DBT and breaking it down into hydroxyl radicals was thought to be responsible for the drop in H_2O_2 concentration [53]. Hydroxyl radicals, which accelerate the conversion of DBT to sulfones, are exceptionally potent oxidizing agents. The H_2O_2 reduction may occur due to a limited quantity of oxidizing chemicals and an extended reaction duration [54].

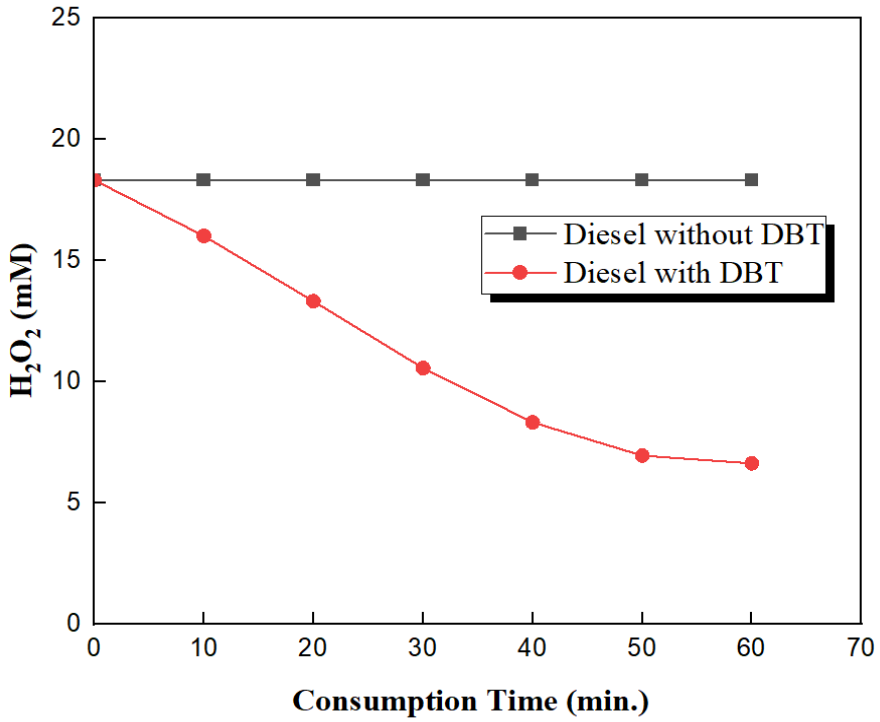

Fig. 8 H_2O_2 Consumption Against Time for 10% Real Diesel without DBT and 10% Real Diesel with DBT, with Electrolyte and Oxygen Flow Rates of 0.25 M KOH, 0.5 V, 15 mL/min, and 1.5 L/min, Respectively, at 20 °C.

3.5.Impact of Different Concentrations of DBT in Diesel Fuel

Figure 9 illustrates the impact of different concentrations of DBT in diesel fuel while maintaining a constant reaction period of one hour. The findings demonstrated a consistent decline in H_2O_2 levels as the concentration of DBT increased. The observed correlation can be ascribed to the oxidant-to-sulfur (H_2O_2/S) ratio. The H_2O_2 to DBT stoichiometric ratio for the oxidation process was two. Multiple factors need utilizing a greater amount of H_2O_2, including challenges in mass transfer between the water and oil phases, H_2O_2 oxidation processes occurring simultaneously, and the thermal breakdown of H_2O_2 into oxygen and water [55]. Full sulfur oxidation cannot be achieved with the weakest quantity of hydrogen peroxide. DBT partially converts to sulfones because a limited supply of oxidants is available [54]. The electrolysis duration is a significant aspect that impacts the oxidative reactions and producing H_2O_2 in situ. It serves as a measure of the effectiveness of the oxidative reaction [56].

3.6.The Effect of Different Electrolyte Concentrations

The electro-production of H_2O_2 relies on the aqueous electrolyte, which helps with the ion transport. Electrochemical oxidation desulfurization does not work with water as a direct ingredient, even if hydroxyl radicals can be generated by oxidizing water at the anode [27]. Fig. 10 displays the influence of different electrolyte concentrations on the in situ production of H_2O_2 with diesel and dibenzothiophene (DBT). Producing H_2O_2 exhibited a linear increase as the electrolyte concentrations rose from 0.25 to 3.0 M. This phenomenon may be ascribed to augmenting the hydroxyl component, which enhances the electrolyte's conductivity and expands the electroactive region. Increased electrolyte concentrations can enhance current efficiency and safeguard the peroxide against future adverse reactions [57]. Elevating the levels of electrolytes might enhance the surface tension, thereby altering the overpotentials [58]. An increase in electrolyte concentration would result in an ionized layer thickness reduction [59]. The concentrations peaked at an electrolyte concentration of 3.0 M. As the concentration of per hydroxyl ions increased, their oxidation rate escalated, while the peroxide generation rate diminished [57].

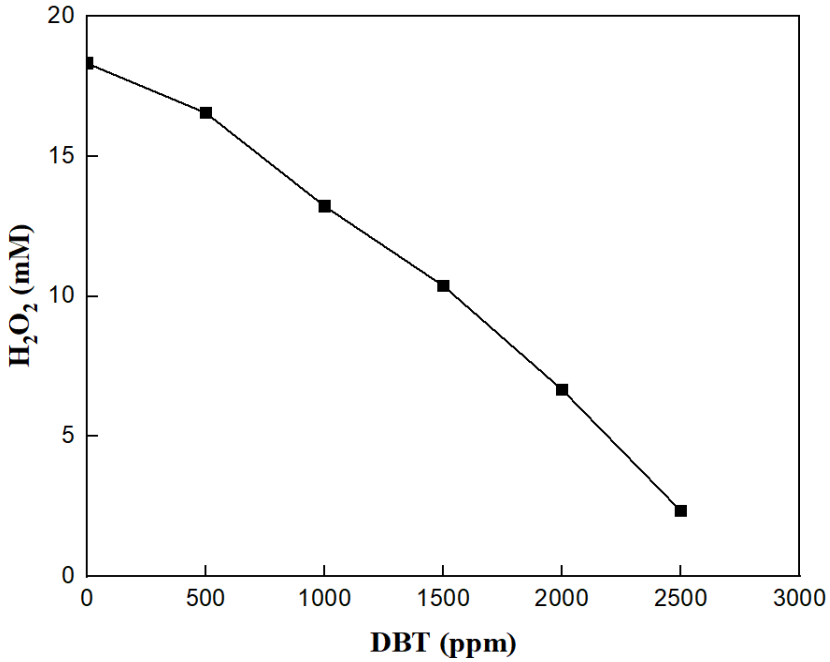

Fig. 9 The Concentration of DBT at a 90/10 Electrolyte to Diesel Ratio Affects the in Situ Formation of H_2O_2 in One Hour.

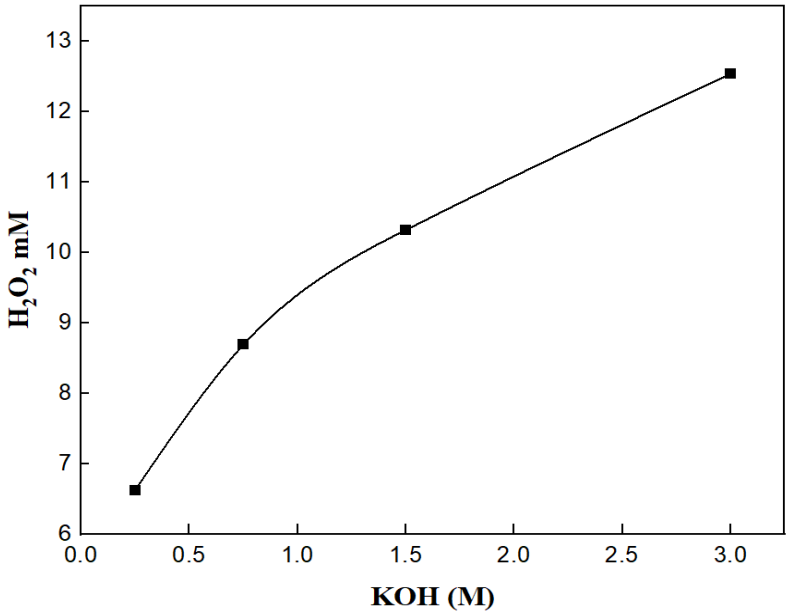

Fig.10 Effect of KOH Concentration on the in-situ Production of H_2O_2 in the Presence of Diesel and DBT After One Hour.

3.7.Effect of Temperature on Dibenzothiophene Rates of Conversions

Seven distinct temperatures were used to conduct the procedure, i.e., 5, 10, 20, 30, 40, 50, and 60 °C, to determine how reaction temperature impacts DBT in situ oxidation. The findings are shown in Fig. 11. In one hour, the DBT conversion rate increased from 20 to 50 °C, from 20.6 to 65.3%, and from 5 to 20 °C, it increased from 8.2 to 20.6%, as shown in Fig. 11. However, it fell below 50 °C. The DBT's oxidation rate increased with the reaction temperature [49]. On the other hand, the DBT conversion ratio dropped when the reaction temperature increased over 50 °C. Reportedly, the following equation's reaction rate would increase at high temperatures, activating H_2O_2 self-decomposition [60].

$$H_2O_2 + HO_2^- \longrightarrow H_2O + O_2 + OH^- \quad (7)$$

Consequently, DBT in situ oxidation was hindered by H_2O_2 breakdown at high temperatures. According to studies, increasing the electrolyte solution temperature accelerates the oxygen evolution reaction and lowers H_2O_2 electrogeneration [26,61].

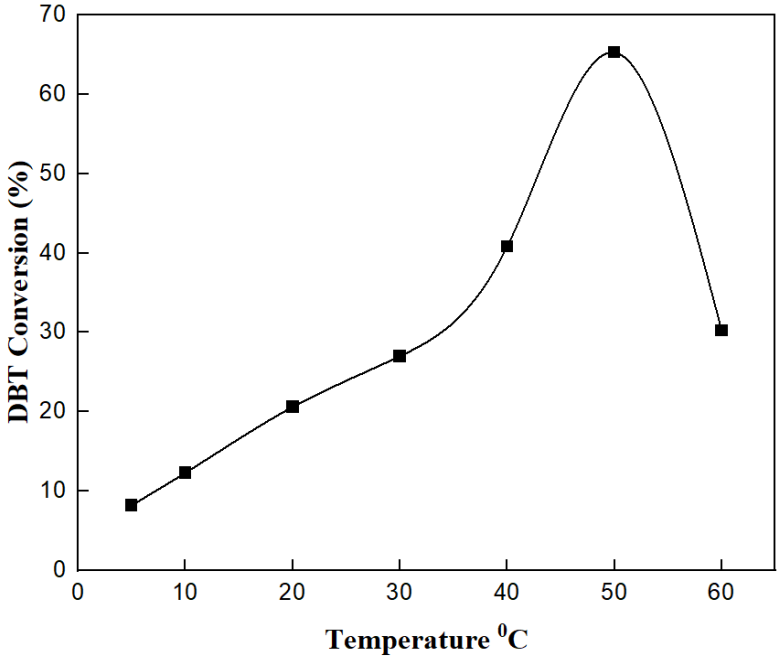

Fig. 11 The Conversion of DBT to a Different Temperature in One Hour.

3.8.Effect of Time on Dibenzothiophene Rates of Conversions

The results of an experiment on how response time affects the conversion rates of DBT dissolved in diesel are shown in Fig. 12, conducted throughout a time range of one to two hours. The steady increase in DBT conversion throughout the first 40 min reached around 20%. After 80 mi., it obtained a conversion rate of around 65.0%; after 2 hours, it reached 100%. It was evident that the sulfur conversion rate increased significantly over the latter 40 minutes compared to the initial 40 minutes because of the DBT low concentration and H_2O_2 high concentration. A sluggish oxidation rate of DBT was observed in the first 40 min due to H_2O_2 generation decrease and, consequently, a slow sulfur conversion rate. Sulfur removal effectiveness dropped with decreasing hydrogen peroxide concentration because the H_2O_2 to DBT ratio was lower than the stoichiometric ratio, around 2:1 for sulfur to H_2O_2. Therefore, the oxidant was in little supply, which might cause DBT to undergo an incomplete conversion to sulfones. A deep sulfur conversion of 100% was accomplished in two hours after an increase in H_2O_2 generation and a high DBT oxidation rate after one hour.

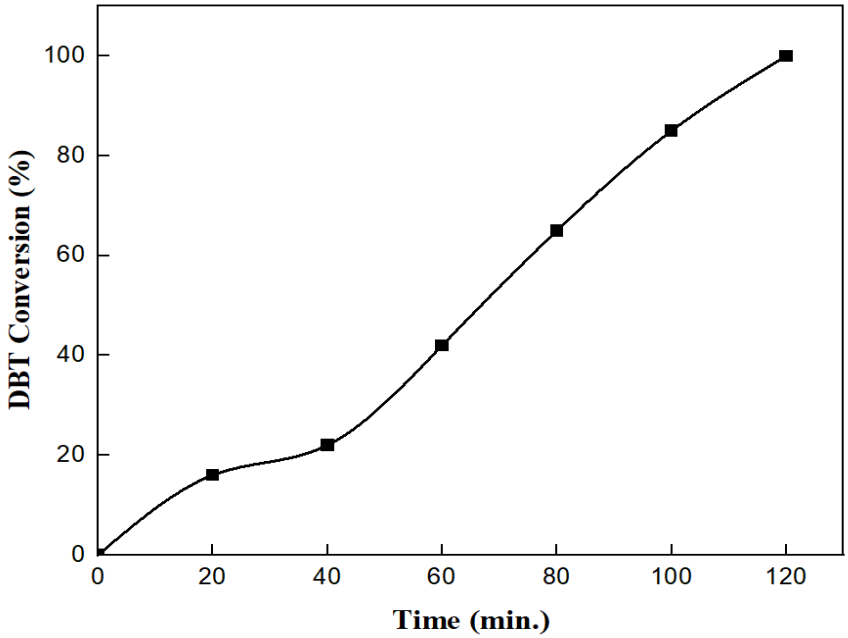

Fig. 12 The Change in DBT Over Time in TBER with the Following Parameters: Running at 20 °C, Electrolyte to Diesel Ratio of 90/10, 0.5 V, 1.5 L/min O2 Flow Rate, and 15 mL/min Electrolyte Flow Rate.

3.9.Oxidation Desulfurization Reaction Kinetics

Investigation of reaction kinetics at various temperatures over time, with a KOH concentration of 0.25 M. The sulfur concentration was tested at various time intervals, i.e., 10, 20, 30, 40, and 50 minutes, and temperatures, i.e., 40, 50, and 60 °C. The response is expressed as follows:

DBT + H_2O_2 $\longrightarrow$ product

$$-\frac{dc_D}{dt} = k\,[H_2O_2]^m[c_D]^n \qquad (8)$$

Eq. (7) states that the reaction rate is ordered with respect to the DBT (n) and H_2O_2 (m) concentrations, where c_D is the concentration of DBT, k is the reaction rate constant, and t is the time. The H_2O_2 term dependent can be ignored because it is abundant [62]. Since the oxidation is often described as a pseudo-first-order reaction, Eq. (8) can be rewritten for n = 1 as follows:

$$-\frac{dc_D}{dt} = k\,[c_D] \qquad (9)$$

with two limits:

$t = 0 \rightarrow c_D = c_o$ and $t = t \rightarrow c_D = c_f$

$$\ln\left(\frac{c_0}{c_f}\right) = -kt \qquad (10)$$

k represents the reaction rate constant, measured in min^{-1}, c_D represents the sulfur concentration, c_f represents the final sulfur concentration, and c_o represents the starting sulfur concentration measured in mol/L. Plotting the natural logarithm of the concentration ratio over initial concentration ($\ln (c_o/c_f)$) against time at various temperatures results in a linear equation with a high coefficient of determination (R_2), which confirms the assumption of kinetics. The reaction rate constant may be determined by calculating the straight lines' slopes, as shown in Fig. 13. The reaction constant and R_2 exhibited a positive correlation with the desulfurization temperature due to their considerable temperature dependence [63]. The reaction rate constants at different temperatures were determined using a power law model and were 0.018, 0.0192, and 0.0195 min^{-1}, respectively. The Arrhenius equation allows for estimating activation energies (AE) for a reaction, given by

$$k = k_o\, exp\,(-AE\,/\,R\,T) \qquad (11)$$

The activation energy (AE) was 4.532 kJ/mol by plotting the natural logarithm of the rate constant (ln k) versus the reciprocal of the temperature (1/T) using data from Fig. 13 and the power law.

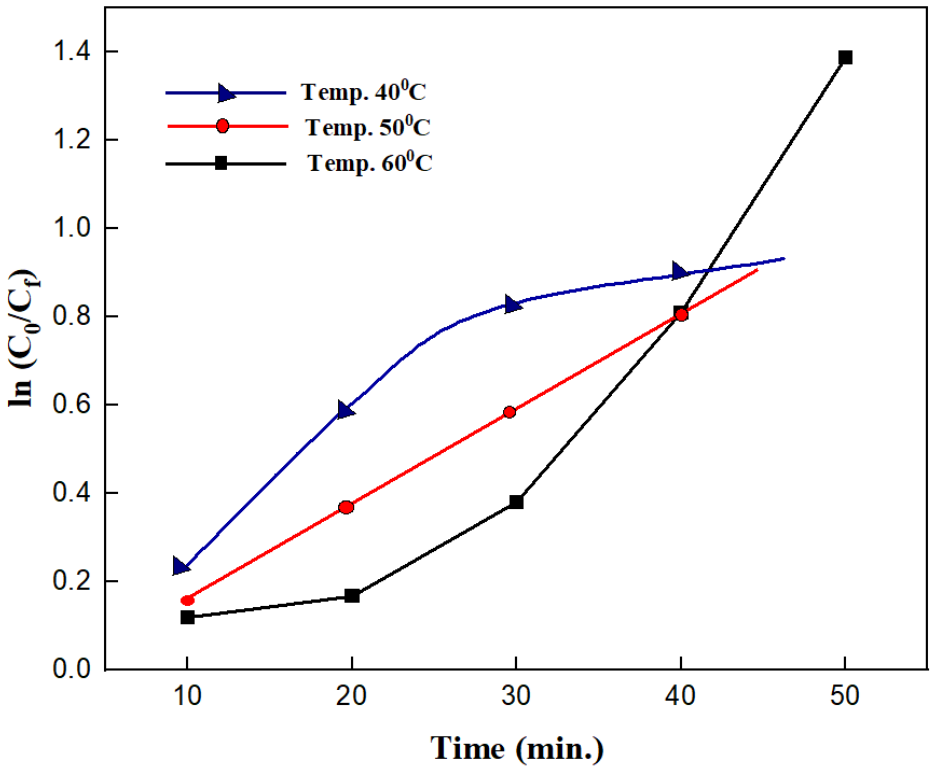

Fig. 13 Correlation between the Natural Logarithm of the Initial Concentration Divided by the Final Concentration and the Duration of Time at the Specified Temperature.

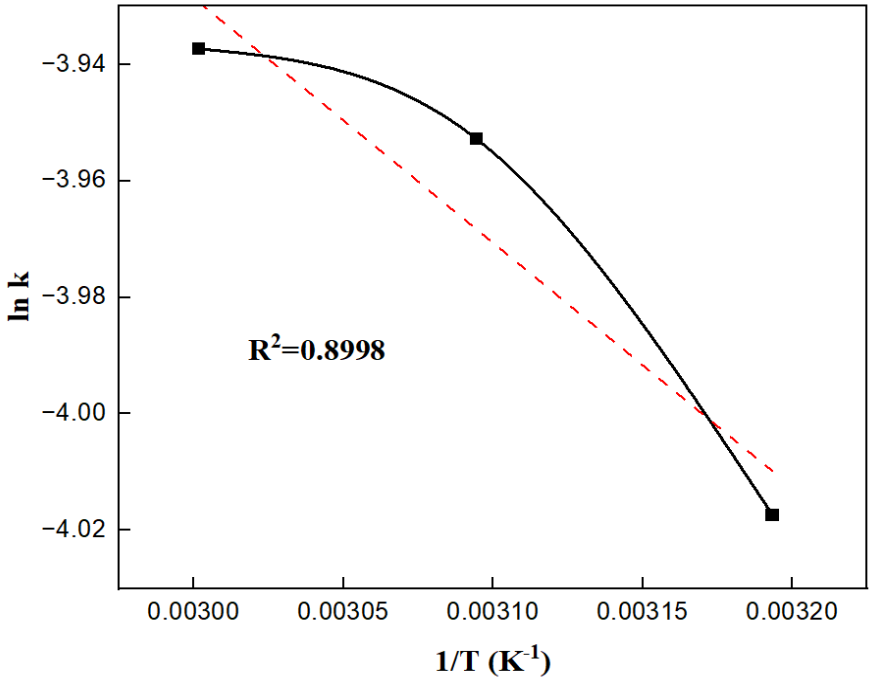

Fig. 14 Influence of Temperature on the Rate Constant of a Reaction.

4.CONCLUSIONS

The present study used MnO_2 nanoparticles as the cathode in a modified trickling bed electrochemical reactor coupled with PTFE to desulfurize Dibenzothiophene (DBT) in diesel fuel. The Co-Precipitation approach effectively produced MnO_2 nanoparticles. The nanoparticles were defined using XRD, SEM, and FTIR methodologies. A study was conducted to evaluate the DBT in situ oxidation in diesel and the electrogeneration of H_2O_2 using a constant voltage of 0.5 V. Introducing 10% diesel into the electrolyte reduced producing H_2O_2 by nearly 50% compared to without diesel, with a concentration of 18.32 mM. Modifying the oil-phase percentages revealed a reduction in peroxide generation, suggesting that the oil phase occupied the active sites. Nevertheless, with the small quantity of hydrogen peroxide generated, a complete conversion efficiency was attained within two hours after the DBT in situ oxidation in the TBER. The TBER has demonstrated a distinctive and pragmatic approach for effectively reducing sulfur emissions in diesel fuel.

REFERENCES

[1] Huirache-Acuña R, Pawelec B, Rivera-Muñoz E, Nava R, Espino J, Fierro. **Comparison of the Morphology and HDS Activity of Ternary Co-Mo-W Catalysts Supported on P-Modified SBA-15 and SBA-16 Substrates**. *Applied Catalysis B: Environmental* 2009;**92**(1-2):168-184.

[2] Stanislaus A, Marafi A, Rana MS. **Recent Advances in the Science and Technology of Ultra Low Sulfur Diesel (ULSD) Production**. *Catalysis Today* 2010;**153**(1-2):1-68.

[3] Jeon H-J, Ko CH, Kim SH, Kim J-N. **Removal of Refractory Sulfur Compounds in Diesel Using Activated Carbon with Controlled Porosity**. *Energy & Fuels* 2009; **23**(5):2537-2543.

[4] Sadeghi M, Hosseini M. **Preparation and Application of Mno2 Nanoparticles/Zeolite Agy Composite Catalyst by Confined Space Synthesis (Css) Method for the Desulfurization and Elimination of Sp and Opp**. *Journal of Nanostructures* 2012;**2**(4):441-455.

[5] Yu X, Han P, Li Y. **Oxidative Desulfurization of Dibenzothiophene Catalyzed by A-Mno_2 Nanosheets on Palygorskite Using Hydrogen Peroxide as Oxidant**. *Rsc Advances* 2018; **8**(32): 17938-17943.

[6] Alheety MA, Al-Jibori SA, Karadağ A, Akbaş H, Ahmed MH. **A Novel Synthesis of Mno2, Nanoflowers as an Efficient Heterogeneous Catalyst for Oxidative Desulfurization of Thiophenes**. *Nano-Structures & Nano-Objects* 2019;**20**:100392.

[7] Alenazi B, Alsalme A, Alshammari SG, Khan R, Siddiqui MRH. **Ionothermal Synthesis of Metal Oxide-Based Nanocatalysts and Their Application Towards the Oxidative**

Desulfurization of Dibenzothiophene. *Journal of Chemistry* 2020;**2020**:1-11.

[8] Subhan S, Yaseen M, Ahmad B, Tong Z, Subhan F, Ahmad W, Sahibzada M. **Fabrication of Mno_2 NPs Incorporated Uio-66 for the Green and Efficient Oxidative Desulfurization and Denitrogenation of Fuel Oils**. *Journal of Environmental Chemical Engineering* 2021; **9**(3):105179.

[9] Kędra-Królik K, Fabrice M, Jaubert J-Nl. **Extraction of Thiophene or Pyridine from N-Heptane Using Ionic Liquids. Gasoline and Diesel Desulfurization**. *Industrial & Engineering Chemistry Research* 2011; **50**(4):2296-2306.

[10] Ali SH, Hamad DM, Albusairi BH, Fahim MA. **Removal of Dibenzothiophenes from Fuels by Oxy-Desulfurization**. *Energy & Fuels* 2009;**23**(12):5986-5994.

[11] Song C, Ma X. **New Design Approaches to Ultra-Clean Diesel Fuels by Deep Desulfurization and Deep Dearomatization**. *Applied Catalysis B: Environmental* 2003;**41**(1-2):207-238.

[12] Alwan HH, Makki HF, Al-Hattab TA. **Preparation, Characterization and, Activity of Como Supported on Graphene for Heavy Naphtha Hydro-Desulfurization Reaction.** *Iranian Journal of Catalysis* 2021;**11**(2):101-111.

[13] Muhammad Y, Rahman AU, Rashid HU, Sahibzada M, Subhan S, Tong Z. **Hydrodesulfurization of Dibenzothiophene Using Pd-Promoted Co–Mo/Al_2O_3 and Ni–Mo/Al_2O_3 Catalysts Coupled with Ionic Liquids at Ambient Operating Conditions**. *RSC Advances* 2019; **9**(18): 10371-10385.

[14] Muhammad Y, Li C. **Dibenzothiophene Hydrodesulfurization Using in Situ Generated Hydrogen over Pd Promoted Alumina-Based Catalysts.** *Fuel Processing Technology* 2011;**92**(3):624-630.

[15] Muhammad Y, Lu Y, Shen C, Li C. **Dibenzothiophene Hydrodesulfurization over Ru Promoted Alumina Based Catalysts Using in Situ Generated Hydrogen**. *Energy Conversion and Management* 2011;**52**(2):1364-1370.

[16] Muhammad Y. **Boosting the Hydrodesulfurization of Dibenzothiophene Efficiency of Mn Decorated (Co/Ni)-Mo/Al_2O_3 Catalysts at Mild Temperature and Pressure by Coupling with Phosphonium Based Ionic Liquids.** *Chemical Engineering Journal* 2019;**375**:121957.

[17] Subhan S, Rahman AU, Yaseen M, Rashid HU, Ishaq M, Sahibzada M, Tong Z. **Ultra-Fast and Highly Efficient Catalytic Oxidative Desulfurization of Dibenzothiophene at Ambient Temperature over Low Mn Loaded Co-Mo/Al_2O_3 and Ni-Mo/Al_2O_3 Catalysts Using Naclo as Oxidant**. *Fuel* 2019;**237**:793-805.

[18] Yaseen M, Shakirullah M, Ahmad I, Rahman AU, Rahman FU, Usman M, Razzaq R. **Simultaneous Operation of Dibenzothiophene Hydrodesulfurization and Methanol Reforming Reactions over Pd Promoted Alumina Based Catalysts**. *Journal of Fuel Chemistry and Technology* 2012;**40**(6):714-720.

[19] Mokhtar WNAW, Bakar WAWA, Ali R, Kadir AAA. **Optimization of Oxidative Desulfurization of Malaysian Euro Ii Diesel Fuel Utilizing Tert-Butyl Hydroperoxide -Dimethylformamide System**. *Fuel* 2015;**161**:26-33.

[20] Gao S, Yu G, Abro R, Abdeltawab AA, Al-Deyab SS, Chen X. **Desulfurization of Fuel Oils: Mutual Solubility of Ionic Liquids and Fuel Oil.** *Fuel* 2016; **173**:164-171.

[21] Shi Y, Zhang X, Liu G. **Adsorptive Desulfurization Performances of Ordered Mesoporous Carbons with Tailored Textural and Surface Properties**. *Fuel* 2015;**158**:565-571.

[22] Martin AB, Alcon A, Santos VE, Garcia-Ochoa F. **Production of a Biocatalyst of Pseudomonas P Utida Cect5279 for DBT Biodesulfurization: Influence of the Operational Conditions.** *Energy & Fuels* 2005;**19**(3):775-782.

[23] Yaseen M, Ullah S, Ahmad W, Subhan S, Subhan F. **Fabrication of Zn and Mn Loaded Activated Carbon Derived from Corn Cobs for the Adsorptive Desulfurization of Model and Real Fuel Oils**. *Fuel* 2021;**284**:119102.

[24] Mehri F, Ghamati M, Rowshanzamir S, Sauter W, Schröder U. **Evaluation of the Membrane Efficiency of Both Nafion and Sulfonated Poly (Ether Ether Ketone) Using Electrochemical Membrane Reactor toward Desulfurization of a Model Diesel Fuel.** *Chemical Engineering Research and Design* 2020;**153**:517-527.

[25] Zhang T, Zhang J, Wang Z, Liu J, Qian G, Wang D, Gong X. **Review of Electrochemical Oxidation Desulfurization for Fuels and Minerals**. *Fuel* 2021;**305**:121562.

[26] Li J-j, Zhou F, Tang X-d, Hu N. **Deep Desulfurization of Kerosene by Electrochemical Oxidation Generating Na_2FeO_4.** *Energy & Fuels* 2016;**30**(10):8091-8097.

[27] Lam V, Li G, Song C, Chen J, Fairbridge C, Hui R, Zhang J. **A Review of Electrochemical Desulfurization Technologies for Fossil Fuels.** *Fuel Processing Technology* 2012;**98**:30-38.

[28] Schucker RC, Baird Jr WC. **Electrochemical Oxidation of Sulfur Compounds in Naphtha Using Ionic Liquids**. The USA, patent No. US 6274026 B1; 2001a: 1-5.

[29] Schucker RC, Baird J. **Electrochemical Oxidation of Sulfur Compounds in Naphtha**. The USA, patent No. US 6338778.

[30] Chen ZD, Gong XZ, Zhi WANG, Wang YG, Zhang S, Xu DP. **Sulfur Removal from Ionic Liquid-Assisted Coal Water Slurry Electrolysis in Kno3 System**. *Journal of Fuel Chemistry and Technology* 2013;**41**(8):928-936.

[31] Wang W, Wang S, Liu H, Wang Z. **Desulfurization of Gasoline by a New Method of Electrochemical Catalytic Oxidation**. *Fuel* 2007a; **86**(17-18):2747-2753.

[32] Wang W, Wang S, Wang Y, Liu H, Wang Z. **A New Approach to Deep Desulfurization of Gasoline by Electrochemically Catalytic Oxidation and Extraction**. *Fuel Processing Technology* 2007b; **88**(10): 1002-1008.

[33] Liu C, Li D, Yang S. **Electrolytic Oxidation of Dibenzothiophene and Diesel Oil in Acetonitrile–Alcohol– Water– Acetic Acid System**. *Petrochem Technology* 2014; **43**(1):24-29.

[34] González–Fuentes MA, Bruno–Mota U, Méndez–Albores A, Teutli–Leon M, Medel A, Agustín R, Méndez E. **Synthesis and Characterization of Uncracked Iro2–Sno2–Sb203 Oxide Films Using Organic Precursors and Their Application for the Oxidation of Tartrazine and Dibenzothiophene**. *International Journal of Electrochemical Science* 2021;**16**(3):210327, (1-22).

[35] Tang XD, Hu T, Li JJ, Wang F, Qing DY. **Deep Desulfurization of Condensate Gasoline by Electrochemical Oxidation and Solvent Extraction**. *RSC Advances* 2015; **5**(66):53455-53461.

[36] Yaseen M, Khattak S, Ullah S, Subhan F, Ahmad W, Shakir M, Tong Z. **Oxidative Desulfurization of Model and Real Petroleum Distillates Using Cu or Ni Impregnated Banana Peels Derived Activated Carbon–Naclo Catalyst–Oxidant System.** *Chemical Engineering Research and Design* 2022;**179**:107-118.

[37] Abdullah GH, Xing Y. **Deep Diesel Desulfurization in Multi-Cell Trickle Bed Electrochemical Reactor with Intensified Hydrogen Peroxide Production over Mno2 Catalyst**. *Petroleum Science and Technology* 2023;**41**(21):2036-2054.

[38] Oloman CW. **Trickle Bed Electrochemical Reactors**. *Journal of The Electrochemical Society* 1979;**126**:1885-1892.

[39] Xiong S, Zhang X, Chu J, Wang X, Zhang R, Gong M, Wu B. **Hydrothermal Synthesis of Porous Sugarcane Bagasse Carbon/Mno2 Nanocomposite for Supercapacitor Application**. *Journal of Electronic Materials* 2018;**47**(11):6575-6582.

[40] Kanha P, Saengkwamsawang P. **Effect of Stirring Time on Morphology and Crystalline Features of Mno2 Nanoparticles Synthesized by Co-Precipitation Method.** *Inorganic and Nano-Metal Chemistry* 2017; **47**(8): 1129-1133.

[41] Kumar H, Manisha SP, Sangwan P. **Synthesis and Characterization of Mno2 Nanoparticles Using Co-Precipitation Technique**. *International Journal of Chemical Engineering* 2013;**3**(3):155-160.

[42] Shaker KS, AbdAlsalm AH. **Synthesis and Characterization Nano Structure of MnO2 Via Chemical Method**. *Engineering and Technology Journal* 2018;**36**(9):946-950.

[43] Barros W, Ereno T, Tavares A, Lanza M. **In Situ Electrochemical Generation of Hydrogen Peroxide in Alkaline Aqueous Solution by Using an Unmodified Gas Diffusion Electrode**. *ChemElectroChem* 2015;**2**(5): 714-719.

[44] Kahattha C, Santhaveesuk S. **Influence of Calcination Temperature on Physical and Electrochemical Properties of Mno2 Nanoparticles Synthesized by Co-Precipitation Method**. *Ferroelectrics* 2019; **552**(1): 121-131.

[45] Ganeshan S, Ramasundari P, Elangovan A, Arivazhagan G, Vijayalakshmi R.

Synthesis and Characterization of MnO2 Nanoparticles: Study of Structural and Optical Properties. *International Journal Scientific Research in Physics and Applied Sciences* 2017;**5**(6):5-8.

[46] Adelkhani H, Ghaemi M, Jafari S. **Novel Nanostructured Mno2 Prepared by Pulse Electrodeposition: Characterization and Electrokinetics**. *Journal of Materials Science & Technology* 2008;**24**(6):857.

[47] Athar T, Hakeem A, Ahmed W. **Synthesis of Mgo Nanopowder Via Non Aqueous Sol–Gel Method**. *Advanced Science Letters* 2012;**7**(1):27-29.

[48] Sudoh M, Kitaguchi H, Koide K. **Polarization Characteristics of Packed Bed Electrode Reactor for Electroreduction of Oxygen to Hydrogen Peroxide**. *Journal of Chemical Engineering of Japan* 1985;**18**(4):364-371.

[49] Huang D, Wang Y, Yang L, Luo G. **Chemical Oxidation of Dibenzothiophene with a Directly Combined Amphiphilic Catalyst for Deep Desulfurization**. *Industrial & Engineering Chemistry Research* 2006;**45**(6):1880-1885.

[50] Sudoh M, Yamamoto M, Kawamoto T, Okajima K, Yamada N. **Effect of Flow Mode of Gas-Liquid Phase in Graphite-Felt Cathode on Electrochemical Production of Hydrogen Peroxide.** *Journal of Chemical Engineering of Japan* 2001;**34**:884-891.

[51] Ranade VV, Chaudhari RV, Gunjal PR. **Chapter 3 - Reaction Engineering of Trickle Bed Reactors.** In: Ranade, VV, Chaudhari, RV, Gunjal, PR, (Eds.), Trickle Bed Reactors. Amsterdam: Elsevier; 2011. pp. 77-116.

[52] Abdullah GH, Xing Y. **Oxidation of Dibenzothiophene in Diesel with in Situ Produced Hydrogen Peroxide**. *Energy & Fuels* 2018;**32**(8):8254-8258.

[53] Haw K-G, Bakar WAWA, Ali R, Chong J-F, Kadir AAA. **Catalytic Oxidative Desulfurization of Diesel Utilizing Hydrogen Peroxide and Functionalized-Activated Carbon in a Biphasic Diesel–Acetonitrile System**. *Fuel Processing Technology* 2010;**91**(9):1105-1112.

[54] Haghighat Mamaghani A, Fatemi S, Asgari M. **Investigation of Influential Parameters in Deep Oxidative Desulfurization of Dibenzothiophene with Hydrogen Peroxide and Formic Acid.** *International Journal of Chemical Engineering* 2013;**2013**(1): 951045, (1-10).

[55] Dehkordi AM, Sobati MA, Nazem MA. **Oxidative Desulfurization of Non-Hydrotreated Kerosene Using Hydrogen Peroxide and Acetic Acid**. *Chinese Journal of Chemical Engineering* 2009;**17**(5):869-874.

[56] Shu C, Sun T, Jia J, Lou Z. **A Novel Desulfurization Process of Gasoline Via Sodium Metaborate Electroreduction with Pulse Voltage Using a Boron-Doped Diamond Thin Film Electrode**. *Fuel* 2013;**113**:187-195.

[57] Oloman C, Watkinson AP. **Hydrogen Peroxide Production in Trickle-Bed Electrochemical Reactors**. *Journal of Applied Electrochemistry* 1979; **9**(1): 117-123.

[58] Staszak K, Wieczorek D, Michocka K. **Effect of Sodium Chloride on the Surface and Wetting Properties of Aqueous Solutions of Cocamidopropyl Betaine**. *Journal of Surfactants and Detergents* 2015; **18**: 321-328.

[59] Brown MA, Goel A, Abbas Z. **Effect of Electrolyte Concentration on the Stern Layer Thickness at a Charged Interface**. *Angewandte Chemie* 2016;**128**(11):3854-3858.

[60] Abel E. **Über Die Selbstzersetzung Von Wasserstoffsuperoxyd.** *Monatshefte für Chemie und Verwandte Teile Anderer Wissenschaften* 1952; **83**:422-439.

[61] Ali MF, Al-Malki A, El-Ali B, Martinie G, Siddiqui MN. **Deep Desulphurization of Gasoline and Diesel Fuels Using Non-Hydrogen Consuming Techniques.** *Fuel* 2006; **85**(10-11): 1354-1363.

[62] Bej SK, Dabral RP, Gupta PC, Mittal KK, Sen GS, Kapoor VK, Dalai AK. **Studies on the Performance of a Microscale Trickle Bed Reactor Using Different Sizes of Diluent**. *Energy & Fuels* 2000;**14**(3):701-705.

[63] Fogler H. ***Elements of Chemical Reaction***. 5th ed., london, UK. Pearson; 2016.